第64卷 第4期 天 文 学 报 Vol. 64 No. 4
2023年7月 ACTA ASTRONOMICA SINICA Jul., 2023

doi: 10.15940/j.cnki.0001-5245.2023.04.011

An Explanation for the Correlation between Type-B QPO Frequency and the Power-law Flux in Black-hole Binaries

HUANG Chang-yin† ZHANG Zi-sheng

(School of Physics and Optoelectronic Engineering, Yangtze University, Jingzhou 434023)

Abstract A positive correlation between the frequency of type-B quasi-periodic oscillations (QPOs) and the associated hard power-law flux has been discovered in a few black hole binaries. The correlation is explained quantitatively based on the Alfven wave oscillation model. The QPO is assumed to be generated by the Alfven wave oscillation in the standard thin Shakura-Sunyaev disk (SSD) at radius with the maximum radiation flux. The power-law flux is calculated based on inverse Compton scattering of soft photons from SSD by a medium of hot electrons in the corona or the base of jet. Both the explicit solutions and numerical results of the correlation between the QPO frequency and the power-law flux with the changing accretion rate are obtained. The modelled correlation fits well into the observed one within reasonable parameter range. The positive correlation could be interpreted by the hypothesis that a stronger magnetic field leads to a higher Alfven wave frequency and a higher electron temperature and therefore a stronger power-law flux. The results suggest that type-B QPOs may be related to the toroidal magnetic activities in the accretion disk or the jet.

Key words accretion, accretion disks, magnetic fields, black hole physics, stars: black holes, X-rays: binaries

Classified index: P142; **Document code:** A

1 Introduction

Complex spectral and timing properties have been observed in Black Hole Binaries (BHBs). During an outburst, three stages are classified, i.e., the hard state, the soft state and the steep power-law state[1] or the intermediate state[2–3]. In the hard state, the spectrum is dominated by a non-thermal power-law component with a typical photon index ∼1.7[1]. In the soft state, the spectrum is commonly described as ∼1 keV thermal emission and can be well interpreted by the standard thin Shakura-Sunyaev Disk (SSD) model[4]. The spectrum of the intermediate state consists of both strong thermal and non-thermal components with typical photon index ∼2.5 and the luminosity is high. The intermediate state is further divided into the Hard InterMediate State (HIMS) and the Soft InterMediate State (SIMS) by Belloni et al.[3].

Received 2022-08-15, revised version 2022-10-10

†hcy@yangtzeu.edu.cn

The HIMS is spectrally dominated by a hard component and with band-limited noise in the Power Density Spectrum (PDS), and the SIMS is spectrally dominated by a soft component and with power-law noise in the PDS[3, 5]. These spectral states appear in counterclockwise order in the q-shaped Hardness-Intensity Diagram (HID) in the sequence of "hard state → HIMS → SIMS → soft state → SIMS → HIMS → hard state"[1, 3, 5–6].

The hard and intermediate states show strong variabilities and quasi-periodic oscillations (QPOs) are usually observed. A narrow peak in the PDS is called a QPO if the quality factor $Q > 2$ (Q is defined as the ratio of the centroid frequency and the full width at half-maximum of the peak)[7]. Low-frequency QPOs (LFQPOs, 0.1–30 Hz) are common in the hard and intermediate state, while high-frequency QPOs (HFQPOs, $>$ 30 Hz) generally appear in the steep power-law state[1, 8] and SIMS[5]. LFQPOs are classified into type A, B and C according to the characteristics of the PDS and phase lags[9–11]. Type-C QPOs are the most common type of LFQPOs with $Q \geqslant 8$ and centroid frequencies of 0.01–30 Hz, which are observed in the hard state and HIMS[11–13]. Type-B QPOs are observed in the SIMS with $Q \geqslant 6$ and typical centroid frequencies of ∼6 Hz or 1–3 Hz[8, 14]. Type-A QPOs are characterized by a weak and broad ($Q \leqslant 3$) peak with centroid frequencies of ∼6–8 Hz, which usually appear in the soft state and SIMS just after the transition from the HIMS[13, 15].

The physical mechanisms of QPOs are not well understood although a variety of models have been proposed. It is believed that HFQPOs are possibly related to the inner region of the accretion disk since the period is comparable to the dynamical time scale of the inner disk[1, 7]. Possible mechanisms for LFQPOs especially type-C QPOs include the relativistic precession[16], the accretion-ejection instability[17], global disk oscillations[18], the oscillation of shocks in accretion flows[19], oscillations of the transition layer between the disk and corona[20], the magnetohydrodynamics (MHD) Alfven wave oscillations in the accretion disk[21], etc. Ingram et al.[22] improved the relativistic precession model for type-C QPOs by considering the Lense-Thirring precession of a radially extended region of the hot inner flow based on the truncated disk model, which sucssefully explained the frequency range and the spectral behavior of type-C QPOs[22–23]. The precession of a small-scale jet is also a possible candidate for the production of LFQPOs, which can naturally explain the high energy, soft lags and energy dependence for frequency and rms (root mean square) of LFQPOs in MAXI J1820+070[24].

Type-B and type-A QPOs are poorly understood. Type-B QPOs are usually observed in the transition from the hard to soft state, the appearance of which indicates the start of the SIMS[5, 15]. They usually appear when BHBs reach their maximum luminosities[14] and occur almost simultaneously with the "jet line"[6]. Therefore, the interpretation of type-B QPOs are important to the study of the states and state transitions of BHBs. Type-B QPOs have completely different properties with type-C QPOs in many aspects[14, 25–26], and there is growing evidence for the jet origin of type-B QPOs[25–27]. Motta et al.[25] analysed the LFQPO data of 14 BHBs and found that type-B QPOs are stronger when the accretion disk is closer to face-on, which supports the hypothesis that type-B QPOs are related to the jet. Russell et al.[28] discovered a compact jet in the SIMS contemporaneous with a type-B QPO in the 2002 outburst of 4U 1543-47. Homan et al.[29] found that a discrete jet ejection launched within ∼2–2.5 hours

after the appearance of a type-B QPO in MAXI J1820+070. Kylafis et al.[30] successfully explained the periodic variation of photon index Γ with the type-B QPO frequency in GX 339-4 based on a precession jet model. The association of type-B QPOs and jet is also evident for H 1743-322 and MAXI J1348-630[31–33].

A strong correlation between the type-B QPO frequency and the power-law flux (hereafter "the QPO-PL relation") has been discovered for a few BHBs[14, 34], which suggests that type-B QPOs may be related to the inverse Compton scattering either from the base of the jet or the corona[14, 25, 34–35]. However, there is a lack of quantitative calculation to interpret this correlation. In this paper, we attempt to explain the QPO-PL relation quantitatively based on the MHD Alfven wave oscillation model[21, 36–39], in which the QPO is produced by the toroidal Alfven wave oscillation due to the radial perturbation of the accreting matter in the inner region of the accretion disk, and the "soft" photons from the disk are inverse Compton scattered by a medium of hot electrons to generate the power-law flux.

The paper is organized as follows. The description of the model is given in Section 2. Then the QPO-PL relation is calculated and compared to the observed one in Section 3. Finally the conclusion is given in Section 4.

2 The model

2.1 The power-law flux

In the relativistic standard thin disk model, the radiation flux per unit disk face area is[40]

$$F = \frac{3GM\dot{M}}{8\pi R_{\rm g}^3} f\,, \tag{1}$$

where G is the gravitational constant, M is the black hole (BH) mass, $\dot{M}$ is the disk accretion rate, and f is a function of dimensionless disk radius $r \equiv R/R_{\rm g}$ ($R_{\rm g} \equiv GM/c^2$ is the gravitational radius, where c is the speed of light) and BH spin a_* given in Ref. [40]. The flux F is assumed to be radiated as blackbody with temperature

$$T(r) = \left(\frac{F}{\sigma}\right)^{1/4} = \left(\frac{3GM\dot{M}}{8\pi R_{\rm g}^3\sigma} f\right)^{1/4}\,, \tag{2}$$

where σ is the Stefan-Boltzmann constant. The radiation intensity is

$$I_{\nu_{\rm i}} = \frac{2h\nu_{\rm i}^3}{c^2}\left[{\rm e}^{\frac{h\nu_{\rm i}}{kT(r)}} - 1\right]^{-1}\,, \tag{3}$$

where h is the Planck constant, k is the Boltzmann constant and $\nu_{\rm i}$ is the frequency of the emitted disk photons.

We assume the soft photons emitted from the surface of the accretion disk are inverse Compton scattered by some hot thermal electrons with temperature $T_{\rm e}$ in a medium above the disk like corona or the base of the jet. If the hot electrons are non-relativistic and the soft photons from the disk satisfy $h\nu_{\rm i} \leqslant h\nu_{\rm s} \ll kT_{\rm e}$ (where $\nu_{\rm s}$ is the maximum frequency of the soft photons), the Comptonized spectrum has a power-law form[41–42]:

$$I_\nu = I_{\nu_{\rm s}}\left(\frac{\nu}{\nu_{\rm s}}\right)^{-\Gamma}\,. \tag{4}$$

The typical value of the spectral index in the SIMS associated with type-B QPOs is $\Gamma \sim 1.5$ (corresponding to photon index ~ 2.5)[1, 5, 34]. We take this value in our calculations.

We take $\nu_{\rm s}$ as the frequency corresponding to the maximum radiation intensity at the hottest part of the disk. By Wien's displacement law, we have

$$h\nu_{\rm s} \approx 3kT_{\rm max} = 3k\left(\frac{3GM\dot{M}}{8\pi R_{\rm g}^3\sigma}\right)^{1/4} f_{\rm max}^{1/4}(a_*)\,. \tag{5}$$

That is

$$\nu_{\rm s} = 6.55\times10^{18} m^{-1/4}\dot{m}^{1/4} f_{\rm max}^{1/4}(a_*)\ {\rm Hz}\,, \tag{6}$$

where $m \equiv M/M_\odot$ ($M_\odot$ is the solar mass), $\dot{m} \equiv \dot{M}/\dot{M}_{\rm Edd}$ ($\dot{M}_{\rm Edd} \simeq 1.4\times10^{18} m\ {\rm g\cdot s^{-1}}$ is the Eddington accretion rate), $T_{\rm max}$ is the maximum temperature of the disk, and $f_{\rm max}(a_*)$ is the maximum value of f, which is a function of a_*.

The observed power-law flux is

$$\begin{aligned} F_{\rm PL} &= \int I_\nu {\rm d}\nu {\rm d}\Omega \\ &= \frac{2h\nu_{\rm s}^{3+\Gamma} R_{\rm g}^2 \cos i (\nu_2^{1-\Gamma} - \nu_1^{1-\Gamma})}{c^2 d^2 (1-\Gamma)} \\ &\quad \int_{r_{\rm in}}^{r_{\rm out}} \left[{\rm e}^{\frac{h\nu_{\rm s}}{kT(r)}} - 1\right]^{-1} 2\pi r {\rm d}r\,, \end{aligned} \tag{7}$$

where d is the distance to the earth and i is the inclination of the line of sight to the normal of the disk. $r_{\rm in} \equiv R_{\rm in}/R_{\rm g}$ and $r_{\rm out} \equiv R_{\rm out}/R_{\rm g}$ are the inner and outer dimensionless radii of the disk respectively. We take $r_{\rm in}$ as the radius of the innermost stable circular orbit $r_{\rm ISCO}$ and $r_{\rm out} = 1000$.

2.2 The QPO frequency

In the Alfven wave oscillation model, an Alfven wave oscillation propagates along the toroidal magnetic field lines in the inner accretion disk due to the perturbation of radial velocity of the accreting matter, and the QPO is produced by the Alfven wave oscillation with frequency[21, 39]

$$\nu_{\rm QPO} = \frac{\omega}{2\pi} = \frac{k' v_{\rm A}}{2\pi}\,, \tag{8}$$

where $k' \sim 2\pi/R$ is the wave number and R is the disk radius at which the oscillation occurs, and $v_{\rm A} = B/\sqrt{4\pi\rho}$ is Alfven speed, where B is the magnetic field and ρ is the mass density of the disk. We adopt the generalized viscosity prescription[43–44]:

$$\frac{B^2}{8\pi} = \alpha P_{\rm gas}^{\mu} P_{\rm tot}^{1-\mu}\,, \tag{9}$$

where α is the viscous parameter, $P_{\rm tot} = P_{\rm gas} + P_{\rm rad}$ is the sum of the gas pressure $P_{\rm gas}$ and the radiation pressure $P_{\rm rad}$, and $0 \leqslant \mu \leqslant 1$ is a free parameter. The magnetic field B and mass density ρ can be obtained by solving the relativistic accretion disk Eqs. (5.6.14) and (5.8.1) in Ref. [45] and Eq. (9). Explicit solutions for special cases and typical values of μ are listed below.

(1) Radiation pressure dominated region ($P_{\rm tot} \approx P_{\rm rad}$, the Rosseland mean opacity $\bar{\kappa} = \bar{\kappa}_{\rm es} = 0.4\ {\rm cm^2\cdot g^{-1}}$, where $\bar{\kappa}_{\rm es}$ is the corresponding opacity by scattering from free electrons).

For $\mu = 0$, we have

$$\begin{aligned} T_{\rm c} &= (5.0\times10^7\ {\rm K})\alpha^{-1/4} m^{-1/4} r^{-3/8} \\ &\quad \mathcal{A}^{-1/2}\mathcal{B}^{1/2}\mathcal{E}^{1/4}\,, \\ \rho &= (1.7\times10^{-7}\ {\rm g\cdot cm^{-3}})\alpha^{-1} m^{-1} \dot{m}^{-2} r^{3/2} \\ &\quad \mathcal{A}^{-4}\mathcal{B}^{6}\mathcal{D}\mathcal{E}^{2}\mathcal{L}^{-2}\,, \\ B &= (6.2\times10^8\ {\rm Gs}) m^{-1/2} r^{-3/4} \mathcal{A}^{-1}\mathcal{B}\mathcal{E}^{1/2}\,, \\ \nu_{\rm QPO} &= (2.9\times10^6\ {\rm Hz})\alpha^{1/2} m^{-1} \dot{m} r^{-5/2} \\ &\quad \mathcal{A}\mathcal{B}^{-2}\mathcal{D}^{-1/2}\mathcal{E}^{-1/2}\mathcal{L}\,, \end{aligned} \tag{10}$$

where $T_{\rm c}$ is the central temperature of the disk. $\mathcal{A}$, $\mathcal{B}$, $\mathcal{D}$, $\mathcal{E}$ and $\mathcal{L}$ are relativistic correction factors given in Ref. [45], which are functions of r and a_*.

For $\mu = 0.5$, we have

$$\begin{aligned} T_{\rm c} &= (3.1\times10^8\ {\rm K})\alpha^{-2/9} m^{-2/9} \dot{m}^{2/9} r^{-2/3} \\ &\quad \mathcal{A}^{-2/9}\mathcal{D}^{-1/9}\mathcal{E}^{1/9}\mathcal{L}^{2/9}\,, \\ \rho &= (2.5\times10^{-4}\ {\rm g\cdot cm^{-3}})\alpha^{-8/9} m^{-8/9} \dot{m}^{-10/9} \\ &\quad r^{1/3}\mathcal{A}^{-26/9}\mathcal{B}^{4}\mathcal{D}^{5/9}\mathcal{E}^{13/9}\mathcal{L}^{-10/9}\,, \\ B &= (6.2\times10^8\ {\rm Gs}) m^{-1/2} r^{-3/4} \mathcal{A}^{-1}\mathcal{B}\mathcal{E}^{1/2}\,, \\ \nu_{\rm QPO} &= (7.5\times10^4\ {\rm Hz})\alpha^{4/9} m^{-19/18} \dot{m}^{5/9} r^{-23/12} \\ &\quad \mathcal{A}^{4/9}\mathcal{B}^{-1}\mathcal{D}^{-5/18}\mathcal{E}^{-2/9}\mathcal{L}^{5/9}\,. \end{aligned} \tag{11}$$

For $\mu = 1$, we have

$$\begin{aligned} T_{\rm c} &= (1.3\times10^9\ {\rm K})\alpha^{-1/5} m^{-1/5} \dot{m}^{2/5} r^{-9/10} \\ &\quad \mathcal{B}^{-2/5}\mathcal{D}^{-1/5}\mathcal{L}^{2/5}\,, \\ \rho &= (0.09\ {\rm g\cdot cm^{-3}})\alpha^{-4/5} m^{-4/5} \dot{m}^{-2/5} r^{-3/5}\mathcal{A}^{-2} \\ &\quad \mathcal{B}^{12/5}\mathcal{D}^{1/5}\mathcal{E}\mathcal{L}^{-2/5}\,, \\ B &= (6.2\times10^8\ {\rm Gs}) m^{-1/2} r^{-3/4} \mathcal{A}^{-1}\mathcal{B}\mathcal{E}^{1/2}\,, \end{aligned}$$

$$\nu_{\rm QPO} = (4039\ {\rm Hz})\alpha^{2/5}m^{-11/10}\dot{m}^{1/5}r^{-29/20} \mathcal{B}^{-1/5}\mathcal{D}^{-1/10}\mathcal{L}^{1/5}\,. \quad (12)$$

(2) Gas pressure dominated region ($P_{\rm tot}\approx P_{\rm gas}$, $\bar{\kappa}=\bar{\kappa}_{\rm es}=0.4\ {\rm cm^2\cdot g^{-1}}$). We have (independent of μ)

$$\begin{aligned} T_{\rm c} &= (1.3\times10^9\ {\rm K})\alpha^{-1/5}m^{-1/5}\dot{m}^{2/5}r^{-9/10} \mathcal{B}^{-2/5}\mathcal{D}^{-1/5}\mathcal{L}^{2/5}\,,\\ \rho &= (61\ {\rm g\cdot cm^{-3}})\alpha^{-7/10}m^{-7/10}\dot{m}^{2/5}r^{-33/20} \mathcal{A}^{-1}\mathcal{B}^{3/5}\mathcal{D}^{-1/5}\mathcal{E}^{1/2}\mathcal{L}^{2/5}\,,\\ B &= (1.6\times10^{10}\ {\rm Gs})\alpha^{1/20}m^{-9/20}\dot{m}^{2/5}r^{-51/40} \mathcal{A}^{-1/2}\mathcal{B}^{1/10}\mathcal{D}^{-1/5}\mathcal{E}^{1/4}\mathcal{L}^{2/5}\,,\\ \nu_{\rm QPO} &= (4039\ {\rm Hz})\alpha^{2/5}m^{-11/10}\dot{m}^{1/5}r^{-29/20} \mathcal{B}^{-1/5}\mathcal{D}^{-1/10}\mathcal{L}^{1/5}\,. \end{aligned} \quad (13)$$

We assume that the QPO is produced at the radius $r_{\rm max}$ where the radiation flux reaches the maximum value. We fit the relationship between $r_{\rm max}$ and a_* based on Eq. (1) and obtain $r_{\rm max}\approx 1.59r_{\rm ISCO}-0.3a_*$. For $a_*=0.5$, substituting $r_{\rm max}$ into Eqs. (10)–(12), we have

$$\begin{aligned} &\nu_{\rm QPO} = (2373\ {\rm Hz})\alpha^{1/2}m^{-1}\dot{m}\,, \quad (\text{for } \mu=0)\,,\\ &\nu_{\rm QPO} = (536\ {\rm Hz})\alpha^{4/9}m^{-19/18}\dot{m}^{5/9}\,, \quad (\text{for } \mu=0.5)\,,\\ &\nu_{\rm QPO} = (163\ {\rm Hz})\alpha^{2/5}m^{-11/10}\dot{m}^{1/5}\,. \quad (\text{for } \mu=1)\,. \end{aligned} \quad (14)$$

The numerical results of B, ρ and $\nu_{\rm QPO}$ at $r_{\rm max}$ as functions of $\dot{m}$ with different parameters (m, a_*, α and μ) are shown in Fig. 1. We see that B and $\nu_{\rm QPO}$ are positively correlated with $\dot{m}$, while ρ changes nonmonotonically with $\dot{m}$, first increases with $\dot{m}$, and then decreases after reaching the maximum where the radiation pressure begins to dominate over the gas pressure. B, ρ and $\nu_{\rm QPO}$ are all anti-correlated with m and positively correlated with a_*. B is insensitive to α and μ. ρ is anti-correlated with α and positively correlated with μ. $\nu_{\rm QPO}$ is positively correlated with α and anti-correlated with μ. The slope of the $\nu_{\rm QPO}$-$\dot{m}$ relation is steeper with a smaller μ.

3 The QPO-PL relation

In order to compare our results to the observed QPO-PL relation in Ref. [34], we adopt the same energy range (3–200 keV) for the power-law flux. Substituting $\nu_1=3\ {\rm keV}/h$, $\nu_2=200\ {\rm keV}/h$, $\Gamma=1.5$ and $\nu_{\rm s}$ in Eq. (6) into Eq. (7), we obtain

$$F_{\rm PL} = 3.13\times10^{39}m^{7/8}\dot{m}^{9/8}\frac{\cos i}{d^2}f_{\rm max}^{9/8}(a_*) \int_{r_{\rm ISCO}}^{1000}\left[{\rm e}^{\frac{h\nu_{\rm s}}{kT(r)}}-1\right]^{-1}2\pi r{\rm d}r\,. \quad (15)$$

Combining Eqs. (14)–(15), we have the $F_{\rm PL}$–$\nu_{\rm QPO}$ relation for different values of $\dot{m}$ and μ as follows (assuming $a_*=0.5$, $i=50^\circ$ and $d=5$ kpc).

(1) $\dot{m}\gtrsim 0.1$, $\mu=0$:

$$F_{\rm PL} = 6.5\times10^{-12}\alpha^{-9/16}m^2\nu_{\rm QPO}^{9/8}\ {\rm erg\cdot cm^{-2}\cdot s^{-1}}\,. \quad (16)$$

(2) $\dot{m}\gtrsim 0.1$, $\mu=0.5$:

$$F_{\rm PL} = 1.2\times10^{-13}\alpha^{-9/10}m^{241/80} \nu_{\rm QPO}^{81/40}\ {\rm erg\cdot cm^{-2}\cdot s^{-1}}\,. \quad (17)$$

(3) $\dot{m}\gtrsim 0.1$, $\mu=1$ or $10^{-5}\lesssim\dot{m}\lesssim 0.1$:

$$F_{\rm PL} = 1.5\times10^{-20}\alpha^{-9/4}m^{113/16} \nu_{\rm QPO}^{45/8}\ {\rm erg\cdot cm^{-2}\cdot s^{-1}}\,. \quad (18)$$

We can see that the slope of the QPO-PL relation becomes steeper with the decreasing accretion rate. Our model predicts $F_{\rm PL}\propto\nu_{\rm QPO}^{45/8}$ with moderate accretion rate.

Numerical results of the modelled QPO-PL relation for different values of m, a_*, α and μ are shown in Fig. 2. We find that the influence of a_* and α on the relation is similar. Both larger values of a_* and α cause the curve move to the right of the graph, while a larger m value causes the curve move up and left. A larger μ value leads to a

steeper correlation when the accretion rate is high. Three curves with different values of μ coincide when the accretion rate is low because $\nu_{\rm QPO}$ is independent of μ when the pressure is dominated by the gas pressure as shown by Eqs. (13)–(14).

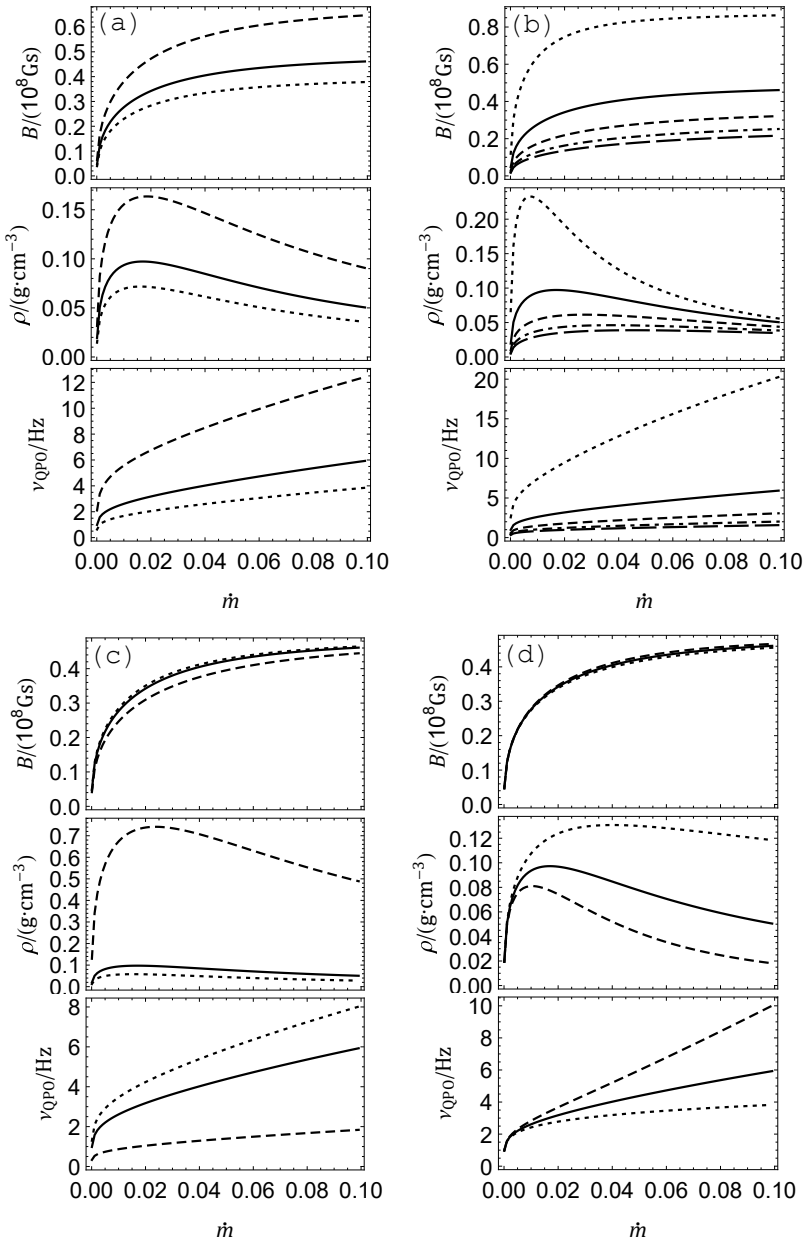

Fig. 1 The curves of B, ρ and $\nu_{\rm QPO}$ as functions of $\dot{m}$. Panel (a): the dashed, solid and dotted lines correspond to $m = 5$, 10, and 15 respectively with fixed $a_* = 0.5$, $\alpha = 0.15$ and $\mu = 0.5$; Panel (b): the long dashed, dot-dashed, dashed, solid and dotted lines correspond to $a_* = -0.9$, -0.5, 0, 0.5, and 0.9 respectively with fixed $m = 10$, $\alpha = 0.15$ and $\mu = 0.5$; Panel (c): the dashed, solid and dotted lines correspond to $\alpha = 0.01$, 0.15 and 0.3 respectively with fixed $m = 10$, $a_* = 0.5$ and $\mu = 0.5$; Panel (d): the dashed, solid and dotted lines correspond to $\mu = 0$, 0.5 and 1 respectively with fixed $m = 10$, $a_* = 0.5$ and $\alpha = 0.15$.

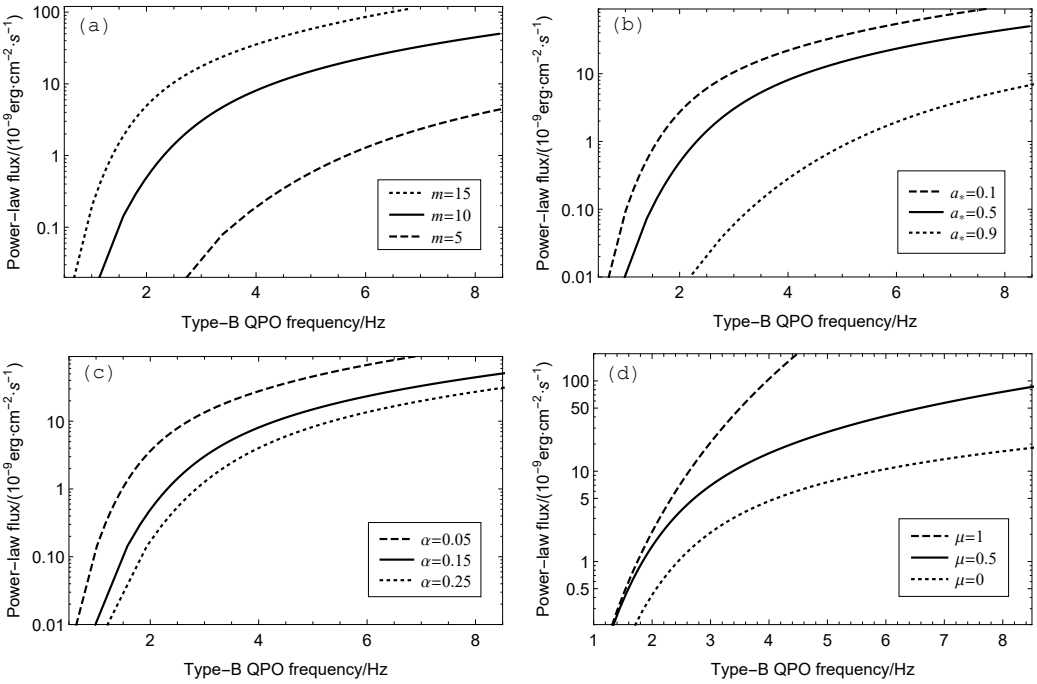

Fig. 2 The theoretical QPO-PL relation with $i = 50°$ and $d = 5$ kpc. The fixed parameters are adopted: (a) $a_* = 0.5$, $\alpha = 0.15$, $\mu = 0.5$; (b) $m = 10$, $\alpha = 0.15$, $\mu = 0.5$; (c) $m = 10$, $a_* = 0.5$, $\mu = 0.5$; (d) $m = 10$, $a_* = 0.5$, $\alpha = 0.15$.

In Fig. 3, we compare the modelled correlation with the observed one (Fig. 8 in Ref. [34]). We adjust the values of α and μ to fit the observed relation with fixed $m = 10$, $a_* = 0.5$, $i = 50°$ and $d = 5$ kpc. The modelled QPO-PL relations fit well into the observed three subgroups with $\alpha \sim 0.1$–0.3 and $\mu \sim 0.2$–0.4. A smaller α value and a larger μ value correspond to the upper subgroup.

As shown in Fig. 8 of Ref. [34], the observed QPO frequencies and the power-law flux for three single sources, namely, GX 339–4, H1743–322 and XTE J1859+226, are well correlated. We fitted the data of these three sources separately as shown in Fig. 4, adopting the source parameters (BH mass, inclination and distance) listed in Tab. 1 of Ref. [34]. For H1743–322, We assume $m = 10$ since its BH mass is unknown and $a_* = 0.2$[46] is taken. For GX 339–4, we adopt $i = 50°$ following Ref. [47] and $a_* = 0.94$[48]. For XTE J1859+226, we take $a_* = 0.5$ since its BH spin is unknown. About the same value $\mu \sim 0.5$ is needed to fit well into the observed correlation of these three sources as shown in Fig. 4.

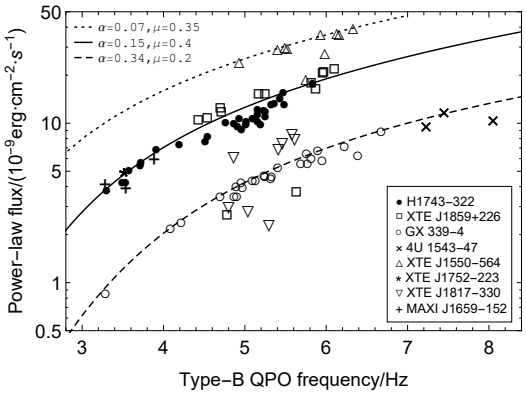

Fig. 3 Comparison of the theoretical QPO-PL relation with the observed QPO frequency and power-law flux for a sample of eight BHBs. The curves are plotted with $m = 10$, $a_* = 0.5$, $i = 50°$ and $d = 5$ kpc. The observational data (taken from Ref. [34], without error bars) of the eight BHBs are shown with different symbols.

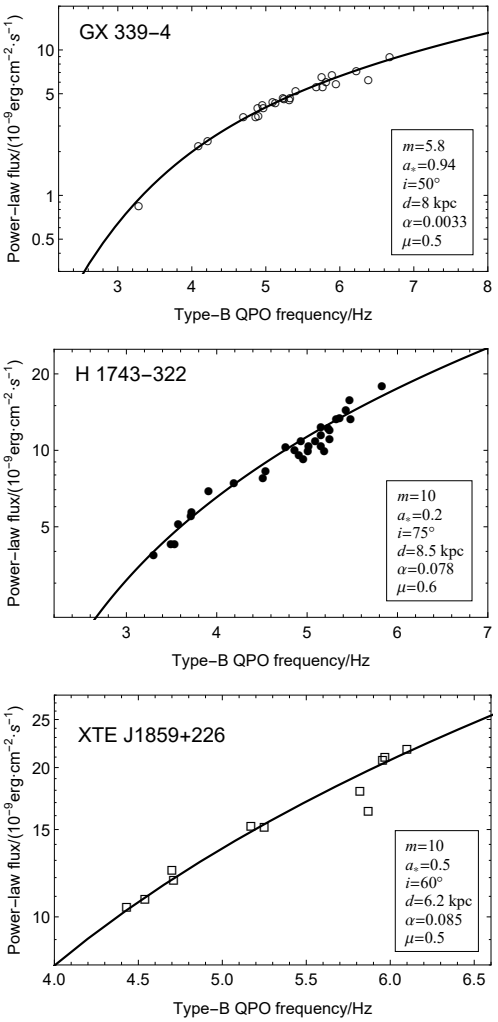

Fig. 4 The QPO-PL relation of GX 339-4, H1743-322 and XTE J1859+226. The curves represent the theoretical relation and different symbols represent the observational data as same as those in Fig. 3.

4 Conclusion

We explain the QPO-PL relation quantitatively based on the MHD Alfven wave oscillation model. The type-B QPO is produced by the Alfven wave oscillation in the inner accretion disk. The power-law flux is calculated based on inverse Compton scattering of soft photons from SSD by a medium of hot electrons. We find that the modelled correlation fits well into the observed one within reasonable parameter range. The results suggest that magnetic fields in the inner region of the accretion disk play a key role in understanding type-B QPO and the associated power-law flux. The hot electrons could be heated by the magnetic reconnection of the tangled small-scale magnetic fields in the inner disk[49–50]. More energy is released in the magnetic reconnection with a stronger magnetic field and hence brings about a higher electron temperature and a stronger power-law flux. The positive correlation between the QPO frequency and power-law flux is expected.

The type-B QPO data used in this paper was observed in the rising phase of outbursts given in Ref. [34]. Data in the decay phase is not included. In order to test whether our model is applicable to type-B QPOs in the decay phase, we also compared our modelled QPO-PL relation with the observed one by Ref. [14] including data both in the rising and decay phase of GX 339–4. However, the modelled relation does not agree with that observed in the decay phase. In the decay phase, both the observed power-law flux and QPO frequency are low. The slope of the correlation is gentle and does not become steep at low accretion rates as in our model (Figs. 2 and 3). In the decay phase, the accretion flow may be different, i.e., with different radiative efficiency, or the corona becomes weak. The association of type-B QPOs and jet is supported by more and more observational evidence[25–33]. We noticed that the toroidal Alfven wave oscillation could also occur in the jet since the toroidal magnetic field will grow with the rotation of the BH (Blandford-Znajek[51] process) or the disk (Blandford-Payne[52] process). The electrons in jet may be heated by the magnetic energy to produce the power-law flux. Therefore, our model is also applicable to the jet origin of LFQPOs. Further investigations are expected in the future work.

ACKNOWLEDGEMENTS We are very grateful to the anonymous referee for his (her) very instructive suggestion for improving our work. C.-Y. Huang thanks J.-L. Qu for his help on the use of the observational data.

Reference

[1] Remillard R A, McClintock L. ARA&A, 2006, 44: 49
[2] Mendez M, van der Klis M. ApJ, 1997, 479: 926
[3] Belloni T M, Homan J, Casella P, et al. A&A, 2005, 440: 207
[4] Shakura N I, Sunyaev R A. A&A, 1973, 24: 337
[5] Belloni T M. States and Transitions in Black-Hole Binaries//Belloni T M. The Jet Paradigm: from Microquasars to Quasars. Berlin Heidelberg: Springer, 2010: 53–84
[6] Fender R P, Belloni T, Gallo E. MNRAS, 2004, 355: 1105
[7] van der Klis M. ARA&A, 2000, 38: 717
[8] Motta S E. AN, 2016, 337: 398
[9] Wijnands R, Homan J, van der Klis M. ApJ, 1999, 526: L33
[10] Remillard R A, Sobczak G J, Muno M P, et al. ApJ, 2002, 564: 962
[11] Casella P, Belloni T, Stella L. ApJ, 2005, 629: 403
[12] Belloni T M, Stella L. SSRv, 2014, 183: 43
[13] Ingram A R, Motta S E. NewAR, 2019, 85: 101524
[14] Motta S, Muñoz-Darias T, Casella P, et al. MNRAS, 2011, 418: 2292
[15] Belloni T M, Motta S E. Transient Black Hole Binaries//Bambi C. Astrophysics of Black Holes. Berlin Heidelberg: Springer, 2016: 61–97
[16] Stella L, Vietri M. PhRvL, 1999, 82: 17
[17] Tagger R, Donahue J, Darrell T, et al. A&A, 1999, 349: 1003
[18] Titarchuk L, Osherovich V. ApJ, 2000, 542: L114
[19] Chakrabarti S K, Manickam S G. ApJ, 2000, 531, L41
[20] Nobili J, Turolla R, Zampieri L, et al. ApJ, 2000, 548: L137
[21] Wang Z Y, Huang C Y, Wang D X, et al. RAA, 2012, 12: 661
[22] Ingram A, Done C, Fragile P C. MNRAS, 2009, 397: L101
[23] Ingram A, Done C. MNRAS, 2011, 415: 2323
[24] Ma X, Tao L, Zhang S N, et al. NatAs, 2021, 5: 94
[25] Motta S E, Casella P, Henze M, et al. MNRAS, 2015, 447: 2059
[26] Stevens A L, Uttley P. MNRAS, 2016, 460: 2796
[27] Fender R P, Homan J, Belloni T M. MNRAS, 2009, 396: 1370
[28] Russell D M, Casella P, Kalemci E, et al. MNRAS, 2020, 495: 182
[29] Homan J, Bright J, Motta S E, et al. ApJ, 2020, 891: L29
[30] Kylafis N D, Reig P, Papadakis I. A&A, 2020, 640: L16
[31] Harikrishna S, Sriram K. 2022, arXiv: 2209.01643
[32] Zhang L, Altamirano D, Uttley P, et al. MNRAS, 2021, 505: 3823
[33] Liu H X, Huang Y, Bu Q C, et al. ApJ, 2022, 938: 108
[34] Gao H Q, Zhang L, Chen Y, et al. MNRAS, 2017, 466: 564
[35] Gao H Q, Qu J L, Zhang Z, et al. MNRAS, 2014, 438: 341
[36] Zhang C. A&A, 2004, 423: 401
[37] Li X D, Zhang C M. ApJ, 2005, 635: L57
[38] Shi C S, Li X D. MNRAS, 2009, 392: 264
[39] Shi C S, Li X D. ApJ, 2010, 714: 1227
[40] Page D N, Thorne K S. ApJ, 1974, 191: 499
[41] Rybicki G B, Lightman A P. AstQ, 1979, 3: 199
[42] Pozdnyakov G B, Sobol I M, Syunyaev R A. ASPRv, 1983, 2: 189
[43] Szuszkiewicz E. MNRAS, 1990, 244: 377
[44] Watarai K Y, Mineshige S. PASJ, 2001, 53: 915
[45] Novikov I D, Thorne K S. Astrophysics of Black Holes// DeWitt C, DeWitt B. Black Holes. New York: Gordon & Breach, 1973: 343–449
[46] Steiner J F, McClintock J E, Reid M J. ApJ, 2012, 745: L7
[47] Tamura M, Kubota A, Yamada S, et al. ApJ, 2012, 753: 65
[48] Miller J M, Reynolds C S, Fabian A C, et al. ApJ, 2009, 697: 900
[49] Di Matteo T. MNRAS, 1998, 299: L15
[50] Liu B F, Mineshige S, Shibata K. ApJ, 2002, 572: L173
[51] Blandford R D, Znajek R L. MNRAS, 1977, 179: 433
[52] Blandford R D, Payne D G. MNRAS, 1982, 199: 883

黑洞双星的B型QPO频率与幂律通量的相关性的解释

黄昌印 张子升
(长江大学物理与光电工程学院 荆州 434023)

摘要 观测表明, 黑洞双星的B型准周期振荡(Quasi-Periodic Oscillation, QPO)频率与幂律通量之间存在正相关性. 试图基于阿尔文波振荡模型定量解释该相关性. 标准薄吸积盘辐射通量极大值处的阿尔文波振荡产生QPO. 标准薄盘上的软光子与冕或喷流基部的热电子介质发生逆康普顿散射产生幂律通量. 通过吸积率的连续变化, 得到QPO频率与幂律通量关系的分析解和数值解. 模拟得到的相关性在合理的参数范围内与观测值相吻合. QPO频率与幂律通量的正相关性可以理解为, 较强的磁场导致较高的阿尔文波频率和较高的电子温度从而得到较高的幂律通量. 结果表明B型QPO可能与吸积盘或喷流中的环向磁场的活动有关.

关键词 吸积, 吸积盘, 磁场, 黑洞物理, 恒星: 黑洞, X射线: 双星